

Large spontaneous-emission enhancements in metallic nanostructures: towards LEDs faster than lasers [Invited]

KOSMAS L. TSAKMAKIDIS,¹ ROBERT W. BOYD,^{2,3} ELI YABLONOVITCH,^{4,5} AND XIANG ZHANG^{1,4,*}

¹Nanoscale Science and Engineering Center, University of California, Berkeley, California 94720, USA

²Department of Physics and Max Planck Centre for Extreme and Quantum Photonics, University of Ottawa, Ottawa, ON K1N 6N5, Canada

³The Institute of Optics and Department of Physics and Astronomy, University of Rochester, Rochester NY 14627, USA

⁴Materials Sciences Division, Lawrence Berkeley National Laboratory, Berkeley, California 94720, USA

⁵Department of Electrical Engineering, University of California, Berkeley, California 94709, USA

*xiang@berkeley.edu

Abstract: Recent progress in the design and realization of optical antennas enclosing fluorescent materials has demonstrated large spontaneous-emission enhancements and, simultaneously, high radiation efficiencies. We discuss here that an important objective of such work is to increase spontaneous-emission rates to such a degree that light-emitting diodes (LEDs) can possess modulation speeds exceeding those of typical semiconductor lasers, which are usually in the range ~20-50 GHz. We outline the underlying physics that enable large spontaneous-emission enhancements in metallic nanostructures, and we then discuss recent theoretical and experimentally promising results, where enhancements larger than a factor of ~300 have been reported, with radiation efficiencies exceeding 50%. We provide key comparative advantages of these structures in comparison to conventional dielectric microcavity designs, namely the fact that the enhancement of spontaneous emission can be relatively nonresonant (i.e., broadband) and that the antenna nanostructures can be spectrally and structurally compatible for integration with a wide class of emitters, including organic dyes, diamond nanocrystals and colloidal quantum dots. Finally, we point out that physical insight into the underlying effects can be gained by analyzing these metallic nanostructures in their equivalent-circuit (or nano-antenna) model, showing that all main effects (including the Purcell factor) can adequately be described in that approach.

©2016 Optical Society of America

OCIS codes: (130.0250) Optoelectronics; (140.5960) Semiconductor lasers; (160.3900) Metals; (230.3670) Light-emitting diodes; (250.5403) Plasmonics.

References and links

1. International Technology Roadmap for Semiconductors, (2007 Edition), <http://www.itrs2.net/itrs-reports.html>
2. A. W. Fang, H. Park, O. Cohen, R. Jones, M. J. Paniccia, and J. E. Bowers, "Electrically pumped hybrid AlGaInAs-silicon evanescent laser," *Opt. Express* **14**(20), 9203–9210 (2006).
3. D. A. B. Miller, "Device requirements for optical interconnects to silicon chips," *Proc. IEEE* **97**(7), 1166–1185 (2009).
4. O. Hess and K. L. Tsakmakidis, "Applied physics. Metamaterials with quantum gain," *Science* **339**(6120), 654–655 (2013).
5. G. Shambat, B. Ellis, A. Majumdar, J. Petykiewicz, M. A. Mayer, T. Sarmiento, J. Harris, E. E. Haller, and J. Vučković, "Ultrafast direct modulation of a single-mode photonic crystal nanocavity light-emitting diode," *Nat. Commun.* **2**, 539 (2011).
6. M. Pelton, "Modified spontaneous emission in nanophotonic structures," *Nat. Photonics* **9**(7), 427–435 (2015).
7. C. Sauvan, J. P. Hugonin, I. S. Maksymov, and P. Lalanne, "Theory of the spontaneous optical emission of nanosize photonic and plasmon resonators," *Phys. Rev. Lett.* **110**(23), 237401 (2013).
8. L. Novotny and N. van Hulst, "Antennas for light," *Nat. Photonics* **5**(2), 83–90 (2011).
9. A. Rose, T. B. Hoang, F. McGuiere, J. J. Mock, C. Ciraci, D. R. Smith, and M. H. Mikkelsen, "Control of radiative processes using tunable plasmonic nanopatch antennas," *Nano Lett.* **14**(8), 4797–4802 (2014).

10. E. F. Schubert, N. E. J. Hunt, M. Micovic, R. J. Malik, D. L. Sivco, A. Y. Cho, and G. J. Zydzik, "Highly efficient light-emitting diodes with microcavities," *Science* **265**(5174), 943–945 (1994).
11. K. Okamoto, I. Niki, A. Shvartsner, Y. Narukawa, T. Mukai, and A. Scherer, "Surface-plasmon-enhanced light emitters based on InGaN quantum wells," *Nat. Mater.* **3**(9), 601–605 (2004).
12. J. B. Khurgin and G. Sun, "Comparative analysis of spasers, vertical-cavity surface-emitting lasers and surface-plasmon-emitting diodes," *Nat. Photonics* **8**(6), 468–473 (2014).
13. M. Moskovits, "Surface-enhanced spectroscopy," *Rev. Mod. Phys.* **57**(3), 783–826 (1985).
14. M. Ringler, A. Schwemer, M. Wunderlich, A. Nichtl, K. Kürzinger, T. A. Klar, and J. Feldmann, "Shaping emission spectra of fluorescent molecules with single plasmonic nanoresonators," *Phys. Rev. Lett.* **100**(20), 203002 (2008).
15. Y. Fang, N. H. Seong, and D. D. Dlott, "Measurement of the distribution of site enhancements in surface-enhanced Raman scattering," *Science* **321**(5887), 388–392 (2008).
16. K. J. Russell, T.-L. Liu, S. Cui, and E. L. Hu, "Large spontaneous emission enhancement in plasmonic nanocavities," *Nat. Photonics* **6**(7), 459–462 (2012).
17. K. Munechika, Y. Chen, A. F. Tillack, A. P. Kulkarni, I. J.-L. Plante, A. M. Munro, and D. S. Ginger, "Spectral control of plasmonic emission enhancement from quantum dots near single silver nanoprisms," *Nano Lett.* **10**(7), 2598–2603 (2010).
18. S. Kühn, U. Håkanson, L. Rogobete, and V. Sandoghdar, "Enhancement of single-molecule fluorescence using a gold nanoparticle as an optical nanoantenna," *Phys. Rev. Lett.* **97**(1), 017402 (2006).
19. P. Anger, P. Bharadwaj, and L. Novotny, "Enhancement and quenching of single-molecule fluorescence," *Phys. Rev. Lett.* **96**(11), 113002 (2006).
20. M. S. Longair, *High Energy Astrophysics*, 2nd ed., vol. 1 (Cambridge Univ. Press, 1992).
21. N. Kumar, *Spontaneous Emission Rate Enhancements Using Optical Antennas* (Technical Reports No. UCB/EECS-2013–107, 2013).
22. M. S. Eggleston, K. Messer, L. Zhang, E. Yablonovitch, and M. C. Wu, "Optical antenna enhanced spontaneous emission," *Proc. Natl. Acad. Sci. U.S.A.* **112**(6), 1704–1709 (2015).
23. M. Staffaroni, J. Conway, S. Vedantam, J. Tang, and E. Yablonovitch, "Circuit analysis in metal-optics," *Photon. Nanostructures: Fundamentals and Applications* **10**(1), 166–176 (2012).
24. J. Zhou, T. Koschny, M. Kafesaki, E. N. Economou, J. B. Pendry, and C. M. Soukoulis, "Saturation of the magnetic response of split-ring resonators at optical frequencies," *Phys. Rev. Lett.* **95**(22), 223902 (2005).
25. N. Engheta, "Circuits with light at nanoscales: optical nanocircuits inspired by metamaterials," *Science* **317**(5845), 1698–1702 (2007).
26. O. Hess, J. B. Pendry, S. A. Maier, R. F. Oulton, J. M. Hamm, and K. L. Tsakmakidis, "Active nanoplasmonic metamaterials," *Nat. Mater.* **11**(7), 573–584 (2012).
27. L. Rogobete, F. Kaminski, M. Agio, and V. Sandoghdar, "Design of plasmonic nanoantennae for enhancing spontaneous emission," *Opt. Lett.* **32**(12), 1623–1625 (2007).
28. J.-J. Greffet, M. Laroche, and F. Marquier, "Impedance of a nanoantenna and a single quantum emitter," *Phys. Rev. Lett.* **105**(11), 117701 (2010).
29. Y. C. Jun, R. D. Kekatpure, J. S. White, and M. I. Brongersma, "Nonresonant enhancement of spontaneous emission in metal-dielectric-metal plasmon waveguide structures," *Phys. Rev. B* **78**(15), 153111 (2008).
30. K. L. Tsakmakidis, A. D. Boardman, and O. Hess, "'Trapped rainbow' storage of light in metamaterials," *Nature* **450**(7168), 397–401 (2007).
31. Q. Gan, Y. Gao, K. Wagner, D. Vezenov, Y. J. Ding, and F. J. Bartoli, "Experimental verification of the rainbow trapping effect in adiabatic plasmonic gratings," *Proc. Natl. Acad. Sci. U.S.A.* **108**(13), 5169–5173 (2011).
32. A. Aubry, D.-Y. Lei, A. I. Fernández-Domínguez, Y. Sonnefraud, S. A. Maier, and J. B. Pendry, "Plasmonic light-harvesting devices over the whole visible spectrum," *Nano Lett.* **10**(7), 2574–2579 (2010).
33. A. I. Fernández-Domínguez, S. A. Maier, and J. B. Pendry, "Collection and concentration of light by touching spheres: a transformation optics approach," *Phys. Rev. Lett.* **105**(26), 266807 (2010).
34. K. L. Tsakmakidis, T. W. Pickering, J. M. Hamm, A. F. Page, and O. Hess, "Completely stopped and dispersionless light in plasmonic waveguides," *Phys. Rev. Lett.* **112**(16), 167401 (2014).
35. T. B. Hoang, G. M. Akselrod, C. Argyropoulos, J. Huang, D. R. Smith, and M. H. Mikkelsen, "Ultrafast spontaneous emission source using plasmonic nanoantennas," *Nat. Commun.* **6**, 7788 (2015).
36. G. M. Akselrod, C. Argyropoulos, T. B. Hoang, C. Ciraci, C. Fang, J. Huang, D. R. Smith, and M. H. Mikkelsen, "Probing the mechanisms of large Purcell enhancement in plasmonic nanoantennas," *Nat. Photonics* **8**(11), 835–840 (2014).
37. G. M. Akselrod, T. Ming, C. Argyropoulos, T. B. Hoang, Y. Lin, X. Ling, D. R. Smith, J. Kong, and M. H. Mikkelsen, "Leveraging nanocavity harmonics for control of optical processes in 2D semiconductors," *Nano Lett.* **15**(5), 3578–3584 (2015).
38. C. Ciraci, R. T. Hill, J. J. Mock, Y. Urzhumov, A. I. Fernández-Domínguez, S. A. Maier, J. B. Pendry, A. Chilkoti, and D. R. Smith, "Probing the ultimate limits of plasmonic enhancement," *Science* **337**(6098), 1072–1074 (2012).
39. G. Walter, C. H. Wu, H. W. Then, M. Feng, and N. Holonyak, "Tilted-charge high speed (7 GHz) light emitting diode," *Appl. Phys. Lett.* **94**(23), 231125 (2009).
40. R.-M. Ma, R. F. Oulton, V. J. Sorger, and X. Zhang, "Plasmon lasers: coherent light source at molecular scales," *Laser Photonics Rev.* **7**(1), 1–21 (2013).
41. T. P. H. Sidiropoulos, R. Röder, S. Geburt, O. Hess, S. A. Maier, C. Ronning, and R. F. Oulton, "Ultrafast plasmonic nanowire lasers near the surface plasmon frequency," *Nat. Phys.* **10**(11), 870–876 (2014).

42. K. E. Dorfman, P. K. Jha, D. V. Voronine, P. Genevet, F. Capasso, and M. O. Scully, "Quantum-coherence-enhanced surface plasmon amplification by stimulated emission of radiation," *Phys. Rev. Lett.* **111**(4), 043601 (2013).
43. P. K. Jha, M. Mrejen, J. Kim, C. Wu, Y. Wang, Y. V. Rostovtsev, and X. Zhang, "Coherence-driven topological transition in quantum metamaterials," *Phys. Rev. Lett.* **116**(16), 165502 (2016).
44. A. Boltasseva and H. Atwater, "Low-loss plasmonic materials," *Science* **331**(6015), 290–291 (2011).
45. U. Guler, A. Boltasseva, and V. M. Shalaev, "Applied physics. Refractory plasmonics," *Science* **344**(6181), 263–264 (2014).
46. R. E. Taylor and J. Morreale, "Thermal conductivity of titanium carbide, zirconium carbide and titanium nitride at high temperatures," *J. Am. Ceram. Soc.* **47**(2), 69–73 (1964).

1. Introduction

There is in recent years a growing realization in the microprocessors and nanoelectronics industries that we are rapidly approaching fundamental speed limits with which logic operations can be performed, primarily owing to excessive energy dissipation and heat generation. It is perhaps surprising that among the three main microprocessing operations, namely logic switching, memory reading/writing, and interconnects for the transfer of electrical signals, it is the latter that by far dissipates most of the energy and is therefore currently the most energy-inefficient aspect of microcomputing. Indeed, in one of its recent reports the International Technology Roadmap for Semiconductors anticipates that 80% of microprocessor power will be consumed by electrical interconnects [1], but this is surely an underestimate since the power dissipated in transistors is used for driving the interconnects. With further device miniaturization the transistor capacitances may shrink but the capacitances of the nanowires used in the interconnects only scale with length (currently ~ 3 pF/cm), leading to an energy cost of typically around 1 pJ/bit.

One of the realistic ways forward that the industry has been considering for quite some time now, is to replace the longer electrical interconnects with optical interconnects, i.e. planar lightwave circuits, that can have minimum power dissipation, ultrahigh bandwidths, and feature wavelength division multiplexing and electrical isolation. Inspired and motivated by the success of photonic technologies in long-haul communications, there is now – in view of the above realizations – a drive to deploy photonics not only for short-distance telecom and datacom systems, but right at the microchip level, co-designing photonic devices and components on silicon together with electronic devices, thereby envisioning digitally assisted and enhanced photonics. The leveraging of high-precision shared Si foundries and its compatibility with advances in packaging, as well as the adoption of Si-photonics research objectives by virtually all major industry players (Intel, IBM, Skorpis, Luxtera, Aurion, Mellanox) strongly indicate that this is a viable research path forward, with anticipated real-life major implications in the forthcoming years. Among the strategies, photonic sources such as III-V's have been bonded to Si, where the III-V materials provide efficient gain while Si defines the laser cavity [2].

In addition to coherent light sources (lasers), there is at present an emerging realization that nanoantenna-enhanced *single-transverse-mode* incoherent sources (energy-efficient light-emitting diodes, LEDs) could also find niche applications in very-short-distance on-chip or chip-to-chip communications. LEDs are already the prime light source for low-cost, short-haul and low bit-rate optical fiber links. The main advantages of LEDs are the absence of threshold current (i.e., more energy-efficient operation), simplicity of the device structure, easier and less expensive fabrication with higher yields compared with lasers, high reliability, simplified biasing arrangements (less complex drive circuitry), no need for thermal or optical stabilization circuits, low temperature sensitivity and good linearity. Typical 'low-power' ring-based modulators operate at an average energy per bit of ~ 500 fJ, while Mach-Zehnder modulators require pJ switching energies. However, in addition to having much wider emission linewidths compared with lasers (e.g., $\Delta\lambda_{\text{LED}} \sim \lambda_0^2 \cdot (3k_B T)/(hc) \sim 100$ nm for a spread of photon energies $\Delta(hf) \sim 3k_B T$, k_B being the Boltzmann constant, at $\lambda_0 = 1310$ nm), which prohibits their use in dense wavelength division multiplexing (DWDM) networks, LEDs have until now been much slower than lasers – operating at typical speeds of 100s of MHz, as compared to 10s of GHz of typical solid-state lasers. For instance, present-day surface- or

edge-emitting LEDs operate efficiently for bit rates of up to ~250 Mb/s. Critically, if these speeds could be improved by a factor of *at least 200* whilst retaining high radiation efficiencies (e.g., at least 50%) and an energy budget per bit of the order of ~1–10 fJ [3], then in light of their aforementioned advantageous characteristics, LEDs could become strong candidates for replacing the much more power-hungry lasers for efficient on-chip (very-short-distance) optical communications for which pulse broadening and dispersion need not necessarily be a key issue [4]. In such a scheme, information could readily be encoded by directly modulating a low-power LED source, overcoming the need for using an external modulator altogether [5]. It is in this respect that optical nanoantennas could potentially be of great aid – as they can allow for dramatic enhancements of spontaneous emission rates, whilst preserving high radiation efficiencies and single-mode operation over broad bandwidths [6–19].

2. Origin and theoretical understanding of the phenomenon

To intuitively understand the physics behind the ability of optical nanoantennas to boost spontaneous emission from molecules and other solid-state emitters (such as organic dyes, colloidal quantum dots, QDs, and diamond nanocrystals), consider a particle with electric charge e being accelerated to a small velocity $\Delta v \ll c$, where c is the vacuum speed of light, over a short period Δt , as illustrated in Fig. 1(a) [20]. Maxwell's equations tell us that the particle, since it accelerates, will emit radiation in the form of an electromagnetic wave, and it is possible – from a simple geometric picture – to calculate the intensity and angular distribution of this radiation. At large distances compared to $\Delta v \times \Delta t$, the field lines are radial and centered in the origin, because the signal (propagating with a finite velocity smaller than c) does not have sufficient time to reach that region. At smaller distances the lines are radial around the new position of the source, as expected, while in-between they are connected in a nonradial way within a small perturbation zone of width $c \times \Delta t$ [see Fig. 1(a)]. From the geometry of Fig. 1(a), we see that the ratio of the angular (E_θ) to the radial (E_r) component of the electric field is: $E_\theta/E_r = \Delta v \cdot t \sin(\vartheta)/(c \cdot \Delta t)$; but we know from Coulomb's law that (in electrostatic units): $E_r = e/r^2$ ($r = ct$), so that: $E_\theta = e \cdot d^2r/dt^2 \cdot \sin(\vartheta)/(c^2 \cdot r)$. Since this component falls-off as only $1/r$ with distance (rather than as $1/r^2$ as is the case for E_r), it will be the only E -field component contributing to the far-field radiation. Using Poynting's theorem, it is now straightforward to show that the total radiated (lost) electromagnetic power over a solid angle $d\Omega = 2\pi \sin(\vartheta) d\vartheta$ is: $P = 2(d^2p/dt^2)^2/(3c^3)$ (in cgs units), or (in SI units): $P = (d^2p/dt^2)^2/(6\pi\epsilon_0 c^3)$, ϵ_0 being the vacuum permittivity and p the electric dipole moment. This is the famous Larmor formula, which – for the case of an oscillating dipole: $p(t) = e \cdot x_0 \cos(\omega t)$ – can more insightfully be re-written as:

$$P = \frac{\pi}{3} \left(\frac{\mu_0}{\epsilon_0} \right)^{1/2} \left(\frac{2x_0}{\lambda} \right)^2 (e\omega)^2. \quad (1)$$

From Eq. (1) we may immediately discern that natural electric dipoles in various media are very inefficient radiators (antennas), because they have sizes $x_0 < 1 \text{ nm} \ll \lambda$, where λ is the wavelength of the emitted radiation (e.g., $\lambda \sim 1000 \text{ nm}$). This also implies that the corresponding *rate* of spontaneous emission ($P/(\hbar\omega)$, \hbar being Planck's reduced constant) is slow, as otherwise (under good radiation-efficiency conditions) more photons would be generated, and P would be large [see Fig. 1(b)]. Hence, usually the light-matter interaction is weak, owing to the large difference between the characteristic wavelengths of light and electrons [21, 22].

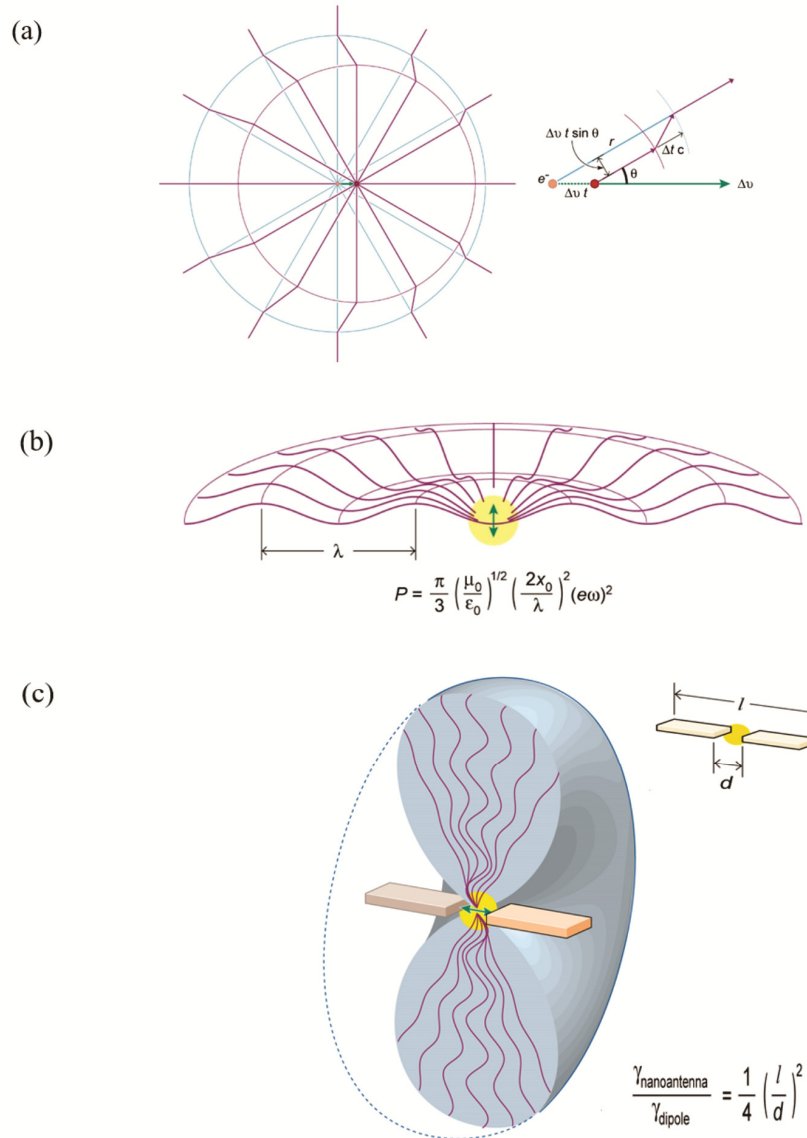


Fig. 1. (a) Schematic illustration of a moving (from left to right) charge e , with the associated emanating electric-field lines. Note the perturbation area between the two circles where the lines are non-radial. (b) Electric dipole oscillating in free space. Because of charge acceleration/deceleration, electromagnetic waves are radiated spherically, with a cycle-averaged power P . (c) When the same dipole is placed parallel between the arms of a nanoantenna, its rate of radiation can be dramatically enhanced, scaling as d^{-2} (as deduced by a simple quasistatic model).

Now consider the case illustrated in Fig. 1(c), where a nanoantenna is placed around the electric dipole. The dipole acts as an oscillating current source, inducing a current I to the nanoantenna plates. Because of conservation of electrostatic energy and charge, the induced electrostatic energy in the nanoantenna, σU (σ and U being, respectively, the induced charge and external voltage in the nanoantenna), will be equal in magnitude (but with an opposite sign) to $e\Phi$, Φ being the dipole potential. Since $U = E \cdot d$ and $\Phi = E \cdot x_0$, E being the parallel electric field in the nanoantenna gap, the induced current will be: $|I| = |d\sigma(t)/dt| = e\omega x_0/d$ [22]. We may, hence, use Eq. (1) to calculate the new spontaneous-emission rate: $\gamma_{\text{nanoantenna}} =$

$R_{\text{rad}} \cdot (e\omega x_0/d)^2/(2\hbar\omega)$, where R_{rad} is the nanoantenna's radiation resistance (e.g., Eq. (1) can also be written as: $P = 0.5I^2R_{\text{rad},0}$, where $R_{\text{rad},0} = (2\pi/3) \cdot (\mu_0/\epsilon_0)^{1/2} \cdot (2x_0/\lambda)^2$ is the free-dipole radiation resistance, and $I = e\omega$ is the equivalent current). Taking the radiation resistance of the short nanoantenna of length ℓ to be: $R_{\text{rad}} = (\pi/6) \cdot (\mu_0/\epsilon_0)^{1/2} \cdot (\ell/\lambda)^2$, we may now readily calculate the nanoantenna-aided spontaneous-emission (SE) rate enhancement:

$$\frac{\gamma_{\text{nanoantenna}}}{\gamma_{\text{dipole}}} = \frac{1}{4} \left(\frac{\ell}{d} \right)^2. \quad (2)$$

Thus, for gaps $d \ll \ell$, the nanoantenna can in principle accelerate spontaneous emission by orders of magnitude. Additional insight is obtained by invoking Fermi's golden rule: $\gamma_{\text{nanoantenna}} = (2\pi/\hbar) \langle m | \mathbf{e} \cdot \mathbf{E} | n \rangle^2 / (\pi\hbar\Delta\omega)$, taking $\epsilon_0 E^2 V_{\text{cav}} = \hbar\omega/2$ for the energy of the vacuum fluctuational field, from where the well-known expression for the Purcell effect, $F_p \sim Q/V$, may readily be deduced [21–23]. Here, it should be pointed out that unless one is dealing with metallic structures close to the surface plasmon frequency and at nanoscopic dimensions (smaller than ~ 25 nm), where the contribution to the impedance by the kinetic inductance dominates ($Z = R + i\omega L_{\text{kin}}$, with $L_{\text{kin}} \sim \text{length}/\text{area}$) [24], an equivalent- RLC -circuit or antenna approach, such as the one above, is sufficient to describe the underlying metal-optics effects [25]. Furthermore, that approach provides a clearer physical insight into and design guidelines for the sought-after SE enhancement. By contrast, if we are closer to the blue region and on truly nanoscopic dimensions, where the electron kinetic inductance starts playing a dominant role, the often-deployed plasmonic-picture analysis becomes more appropriate.

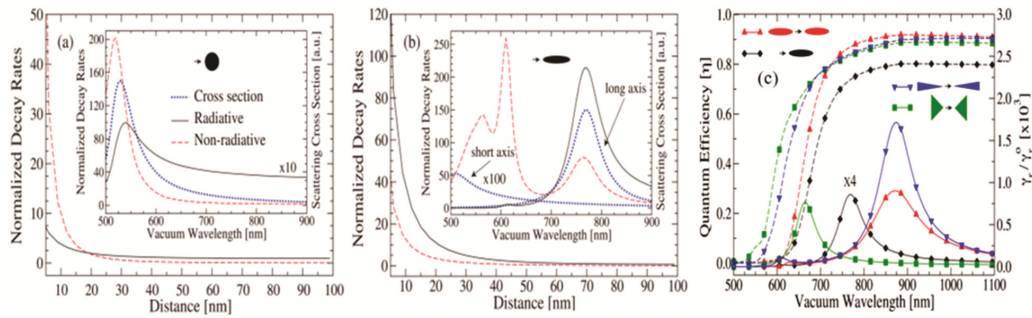


Fig. 2. Normalized decay rates for an emitter placed in the near-field of a gold (a) spherical and (b) elliptical nanoparticle. In both cases, the area of the particle is the same. For (a) the emission wavelength is 535 nm, whereas for (b) it is 770 nm. In both (a) and (b), the insets show the normalized decay rates as a function of the wavelength, for the case when the emitter is 3 nm away from the nanoparticle. (c) Normalized radiative decay rates (solid lines) and radiation efficiencies (dashed lines) for various Au nanoantennae configurations, where in all cases the area of the structure remains the same. [From L. Rogobete et al., Opt. Lett. 32, 1623 (2007)]

Since in LEDs (which, unlike lasers, are non-threshold devices, with no relaxation oscillations in the photon and population dynamics [4, 26]) the modulation bandwidth is proportional to the spontaneous-emission rate, one might realistically hope based on the above analysis to attain LED speeds approaching hundreds of GHz (from hundreds of MHz currently) with a suitably designed nanoantenna structure enclosing a fluorescent material.

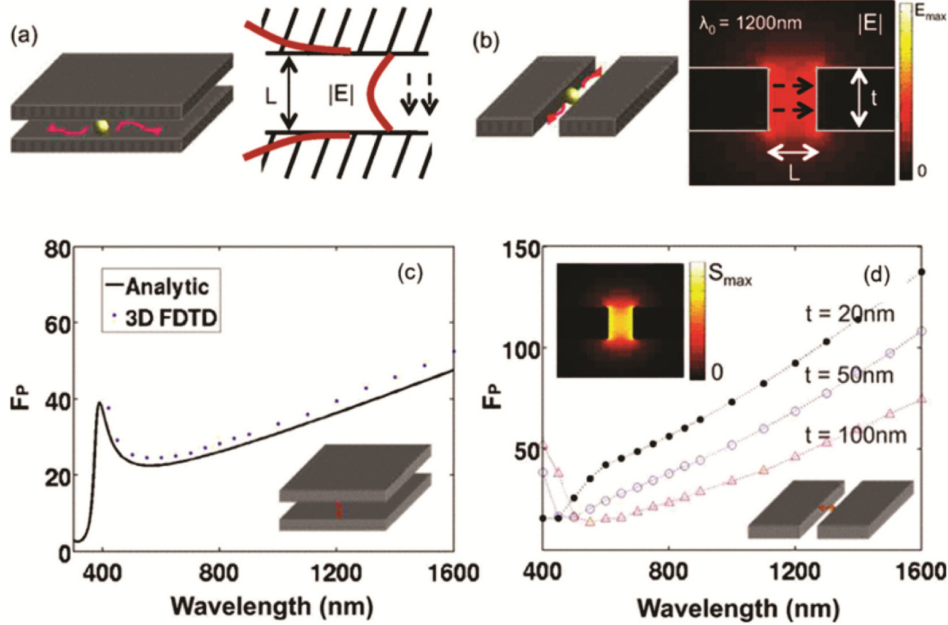


Fig. 3. (a) Schematic illustration of a metal-dielectric-metal slab waveguide, where shown in the middle is an emitted coupling to the supported waveguide modes. The right part shows the discontinuous electric-field profile of the fundamental mode. The dotted arrows indicate that the electric field is primarily directed perpendicularly to the two media interfaces, somewhat similarly to a capacitor. (b) Same as in (a) but now for a slot waveguide, where the width of the metallic layers is finite. (c) Calculated SE-enhancement factor versus wavelength, for the structure of (a). (d) Same as in (c), but now for the structure of (b). [From Y. C. Jun et al., Phys. Rev. B 78, 153111 (2008)]

An impetus in the pursuit of nanoantenna-based designs for enhancing spontaneous emission emerged after it was realized that this route allows not only for drastically increasing radiative decay rates – by up to three orders of magnitude – but also for maintaining (antenna radiative) efficiencies above 50% in the near-infrared regime [27]. Here, the key idea is to use a suitably shaped (e.g., elliptical) nanoparticle [see Fig. 2(a)] or nanoantenna [see Fig. 2(c)] to push the resonant response into the near-infrared (rather than the visible) where the dissipative losses for noble metals, such as gold, are considerably smaller – and thereby radiative decay can dominate over non-radiative channels. Figure 2(b) shows that an emitter coupled to an *elliptical* nanoparticle is characterized (at a wavelength of around 770 nm) by a radiative decay rate γ_R that far exceeds the non-radiative rate γ_{NR} . Similarly, Fig. 2(c) shows that the radiation efficiency (yield) of an emitter coupled to the “hotspot” region of a bow-tie gold nanoantenna exceeds 80%, with the radiation spontaneous-emission enhancement itself being of the order of ~ 1700 . This enhancement is a direct result of the large field-enhancement in the region between the two particles of the nanoantenna. It should here be noted that for practical applications – particularly for ultrafast LEDs – the Purcell factor is not the only parameter of interest because, in general, a large part of the energy extracted from the emitter can be converted into heat in the nanoantenna [28]. Thus, the radiative yield, $\eta = \gamma_R / (\gamma_R + \gamma_{NR})$, is also a key parameter. If η is small, then in light of the fact that the power output of LEDs is smaller compared to lasers, the radiated LED power might be insufficient for being detected in state-of-the-art photodetectors used in on-chip optical interconnects [5].

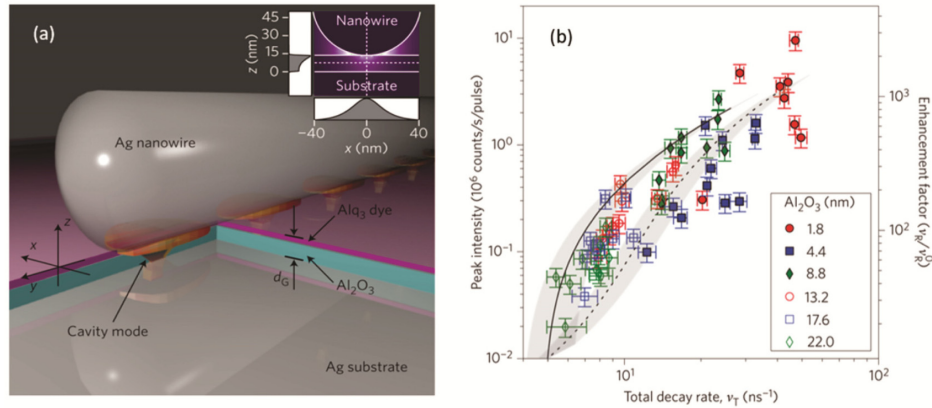


Fig. 4. (a) Schematic illustration of a silver (Ag) nanowire on top of a silver substrate. Between the nanowire and the substrate there is a nm-thickness (d_G) spacer made of a dielectric, Al_2O_3 , coated with a fluorescent organic dye, Alq_3 . The upper inset shows the electric-field profile of the nano-confined supported mode. (b) Measured peak fluorescence intensity as a function of the total emission-decay-rate for various thicknesses of the dielectric (Al_2O_3) spacer. Point symbols are measurement data, the solid line is the theoretical prediction, and the shaded bands indicate the 95%-confidence region of the measurement of the bulk emission rate of Alq_3 . Also shown at the right-hand vertical axis is the corresponding SE-enhancement factor. [From K. J. Russell et al., Nature Photon. 6, 459-462 (2012)]

An interesting point to note is that this type of antenna nanostructures, in principle, allows for relatively *nonresonant* (i.e., broadband) Purcell effects, arising from the associated deep-subdiffraction mode volumes. Indeed, a simple analysis for the 2D slot metal-dielectric-metal (MDM) structure of Fig. 3(b) shows that the SE-enhancement factor is given by [29]: $\text{SE}_F = [3/(4\pi)] \cdot [c/(nv_g)] \cdot [(\lambda_0/n)^2/A_{\text{eff}}]$, where v_g is the group velocity of the mode to which spontaneous emission (SE) couples, and A_{eff} is the mode's 2D effective surface. Hence, there are two contributions to the SE-enhancement: first, a reduction of the mode's group velocity, which usually happens around a specific frequency where the band is flat, i.e. it is a resonant, narrowband contribution; and second, a *nonresonant* contribution, which arises solely from a reduction of the mode's effective area. Both of these contributions associated with 1D and 2D MDM nanoguides are clearly visible in Figs. 3(c)-3(d). In the nonresonant region, although the group-velocity reduction is not large, the normalized mode area $A_{\text{eff}}/(\lambda_0/n)^2$ decreases almost linearly with wavelength, giving rise to SE-enhancements that can readily be of the order of hundreds. We note in passing that the group-velocity reduction too can be nonresonant and broadband in suitably designed structures, such as linearly- or cylindrically- or spherically-tapered nanophotonic structures [30–33]. The group-velocity slowing-down factors can also be extremely large, reaching values of $\sim 10^7$ in principle [34]. Finally, it is to be noted that in the nonresonant regime ($\lambda_0 > \sim 800$ nm in Figs. 3(c)-3(d)) the mode is progressively more tightly confined in the lossless core (dielectric) region, making it less lossy – i.e., the nonresonant SE-enhancement is also associated with higher internal quantum efficiency. Since the mode is confined mainly in the dielectric region, the resulting bright fluorescence can also eventually butt-couple to a standard dielectric waveguide.

3. Recent experimental progress

How close are we to attaining such large SE-enhancement factors in the high-radiation-efficiency limit? Before we proceed with overviewing recent experimental advances in that direction, it should be pointed out that in designing nanoantenna-based SE-enhancement structures the following two issues should always be considered: First, in acting as a nanoantenna, the metallic nanostructure may improve the efficiency of excitation and collection of the fluorescence, potentially giving the erroneous impression that this enhanced collection might be the result of SE-rate enhancement. Second, as remarked before, it is crucial that the

radiative-emission rate, γ_R , is enhanced more strongly than the non-radiative emission rate, γ_{NR} . The latter usually arises from coupling of the fluorescent emission to the metallic-medium layers, where it is quenched, or by inherent defects in the active material. Thus, it is highly desirable that the radiation efficiency, η , is engineered to be larger than 50%.

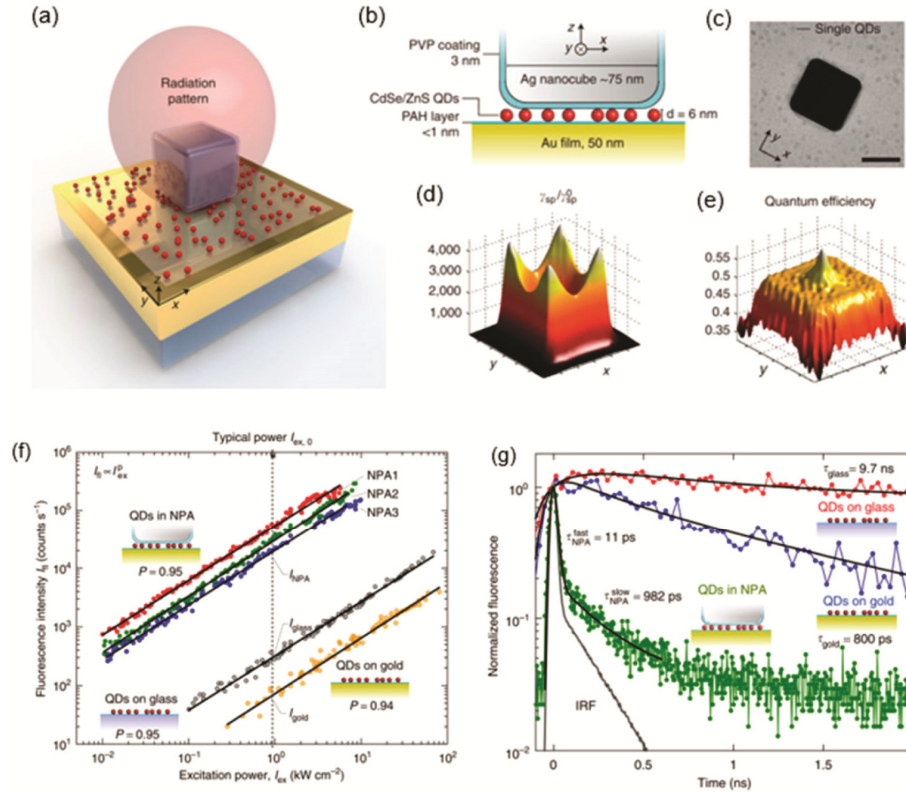


Fig. 5. (a) Three-dimensional illustration of the nanopatch-antenna (NPA), together with its associated far-field directional radiation pattern. (b) Cross-sectional schematic of the NPA, showing a silver nanocube on top of an Au film, separated by a 1 nm polyelectrolyte spacer layer and a sparse layer of ~ 6 nm diameter CdSe/ZnS QDs. (c) Transmission electron microscopy image of a silver nanocube and QDs; scale bar, 50 nm. (d, e) Simulated spatial maps of (d) spontaneous emission rate enhancement and (e) radiative quantum efficiency for a vertically oriented QD dipole situated in the gap between the nanocube and the Au film. (f) QD fluorescence intensity as a function of average incident laser power in three cases: on a glass slide, on an Au film and coupled to individual NPAs (NPAs 1–3). The solid lines are fits to a power law, with the power exponent, P , showing a nearly linear scaling. (g) Normalized time-resolved fluorescence of QDs on a glass slide (red) compared with QDs on an Au film (blue) and coupled to a single NPA (green). The instrument response function (IRF) is also shown. Fits to the data are shown in black. [From T. B. Hoang et al., Nature Commun. 6, 7788]

Figure 4(a) illustrates an example of a nanostructure where very large radiative emission enhancements have been observed, but probably with efficiencies smaller than 50% [16]. It consists of a silver (Ag) nanowire sitting on top of a silver substrate. Between them there is a dielectric spacer coated with a fluorescent organic dye. The peak intensity of the fluorescence emission, α_0 , is related to the number of excited dye molecules N_0 , the collection efficiency q , and the radiative rate, γ_R , by the relation: $\alpha_0 = N_0 q \gamma_R$, which allows to relate enhancements in the peak intensity to enhancements of the radiative decay rates. Figure 4(b) shows that SE-enhancements achieved in this structure are of the order of $\sim 10^3$ (relative to the SE rate in the bare fluorescent dye). Importantly, the authors of [16] calculated that for spacer thicknesses smaller than approximately 7 nm, and with a 2 nm-thick buffer between the dye and the

nanowire, the emission rate into the tightly confined gap mode becomes very large but most of the emission is dissipated as heat. It is to be noted that an additional advantage of these metal-based optical nanostructures is that they lend themselves to integration with emitters that are normally incompatible, either spectrally or structurally, with dielectric-microcavity designs, such as organic dyes and diamond nanocrystals.

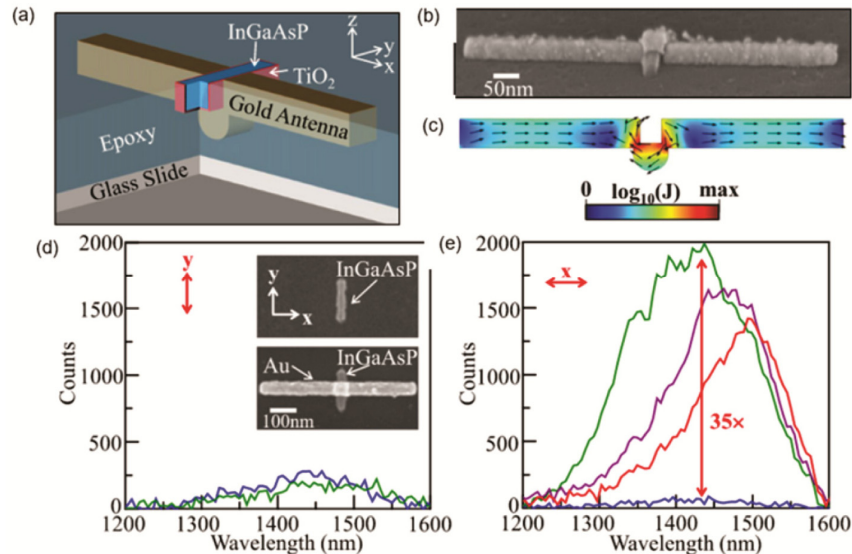


Fig. 6. (a) Schematic illustration of the arch-antenna-coupled InGaAsP nanorod, isolated by TiO₂, and embedded in epoxy. (b) Scanning electron microscope (SEM) image of the nanoantenna structure. (c) Simulated current density profile in the nanoantenna, showing the antiparallel current in the arch compared with the arms of the antenna. (d) Optical emission for *E*-field polarized in the *y*-direction, for bare nanorod (blue) and antenna-coupled nanorod (green). (Inset) Top-down SEM image of antenna-coupled and bare nanorod. (e) Optical emission for *E*-field polarized in the *x*-direction, for a bare nanorod (blue) and from nanorods coupled to different antenna lengths: 400 nm (green), 600 nm (purple), and 800 nm (red) in length. [From M. S. Eggleston et al., Proc. Nat. Acad. Science 112, 1704-1709 (2014)]

A further recently-reported structure consists of nanopatch antennas (NPAs) coupled to colloidal quantum dots (QDs) [9, 35–38]. In this setup, silver nanocubes are placed above a gold film, from which they are separated by a 5–15 nm thin spacer; the colloidal QDs are placed inside this high-field-intensity spacer region, as shown in Figs. 5(a)–5(d). The dominant field-component is normal to the gap and is enhanced by (up to) a factor of more than 100, which is argued to be sufficient to induce SE-rate enhancements exceeding several hundred – thereby anticipating emission rates of ~ 90 GHz, which should correspond to SE lifetimes of less than 11 ps. However, it is at the moment unclear whether the antenna currents concentrated in the gap region can strongly contribute to radiation (instead of heat dissipation). This nanopatch-antenna geometry could, further, readily be tuned from the visible to the near-infrared by suitably adjusting the side-length of the nanocubes and the thickness and refractive index of the gap material, and since it deploys metals it lends itself naturally to placing electrodes for electrical pumping and direct demonstration of high-speed, efficient LED modulation – an obvious next objective. It should be mentioned in passing that a recent work has demonstrated high-speed (7 GHz) LEDs using a bipolar junction to sweep away carriers that do not recombine sufficiently fast [39]. Also, room-temperature modulation of LEDs based on photonic crystal cavities has resulted in speeds of up to 10 GHz, although with output powers of the order of tens to hundreds of pW (at μ W bias levels), indicating an efficiency of $\sim 10^{-5}$ [5]. It should here be noted that despite advanced techniques to fabricate and tune high-*Q* cavities, including micropillar cavities,

microtoroid resonators and photonic crystal cavities, experimental values of spontaneous-emission enhancement factors in dielectric optical cavities are presently limited to less than 100. In addition, these systems are typically narrowband and often require low temperatures, i.e., they are not ideal systems for controlling broadband emission from room-temperature emitters [35].

Substantial SE rate enhancements have also recently been reported in arch-antenna-coupled InGaAsP nanorods (acting as the spontaneous light-emitting material), as shown in Fig. 6 [22, 23]. Here, the metallic arch acts as an effective inductor across the gap to reduce the effective gap capacitance of the antenna, which is otherwise responsible for shorting out the currents induced in the nanoantenna's arms before they can 'see' the radiation resistance. Spontaneous emission intensity enhancements of 35 have thus been attained (for incident E -field polarization parallel to the nanoantenna gap), corresponding to SE-rate speedups of around 115, for antenna gap spacing $d = 40$ nm. The enhancement is spectrally broad, spanning almost 200 nm of vacuum wavelength, indicating an antenna Q -factor of the order of 5 – i.e. very small, as it should be for a good antenna. In this configuration, too, the resonance frequency can readily be tuned (redshifted) by lengthening the nanoantenna arms. Further improvements are anticipated by fabricating shorter nanorods to allow more carriers to diffuse to the nanoantenna hotspot, and by improved-surface structures to reduce the detrimental role of carrier surface recombination.

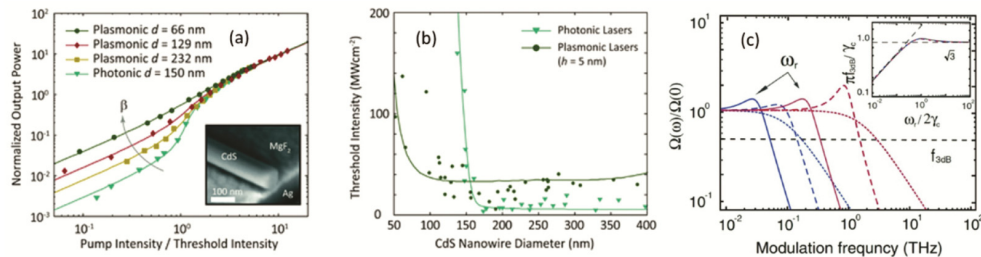


Fig. 7. (a) Dependence of the measured output laser power on the pump intensity, for plasmonic (Ag) and photonic nanowire lasers. For higher Purcell factors, leading to higher β coupling factors, the threshold kink progressively smooths out. (b) Dependence of measured threshold intensity on the nanowire diameter, for plasmonic and photonic lasers. The experimental data points have been obtained by measuring the pump intensities at which coherent peaks started to appear in the output spectrum. (c) Theoretically calculated small-signal modulation response of one-dimensional (red curves) and two-dimensional (blue curves) plasmonic nanolasers, at telecommunication wavelengths ($\omega = 0.83$ eV, $\lambda \sim 1.5$ μm) and for progressively increasing pump rates (solid to dashed to dotted lines). The inset shows the calculated 3 dB modulation bandwidth as a function of the relaxation-oscillations frequency, ω_r , which follows a universal dependence for all cases (see main text). [From D. A. Genov et al., Phys. Rev. B 83, 245312 (2011); and R. F. Oulton et al., Nature 461, 629-632 (2009)]

As a final remark, it should be noted that the large SE-enhancements in antenna nanostructures might also be of interest for creating relatively low-threshold nanolasers – except that the optimization is, in that case, quite different. Indeed, while overall optical losses are, in a sense, beneficial in designing a good antenna (since the Q -factor of a good antenna should be of the order of unity to allow for good in-/out-coupling of radiation to the antenna), they are disadvantageous for lasers, which require small total (dissipative + radiative) losses for low-threshold operation [4, 26, 40–43]. Here, a key quantity of interest is the fraction of spontaneous emission coupling to the preferred lasing mode – the, so-called, β factor. For electrically-pumped semiconductor nanolasers, in particular, the threshold pump rate is $J_{\text{th}} = \gamma_{\text{tot}}/\beta$, where γ_{tot} is the total cavity-loss rate, including both dissipative and radiative cavity losses. In conventional semiconductor lasers, the β factor is very small (typically, $\beta \sim 10^{-3} - 10^{-4}$), and thus low cavity losses are required for J_{th} to not be unrealistically large. By contrast, in optical antennas the β factor can be of the order of unity, thereby allowing for higher cavity losses without necessarily increasing significantly the

lasing-threshold requirements. Indeed, as Fig. 7(b) shows, the threshold pump-intensity for plasmonic nanowire lasers ($\sim 20\text{-}50 \text{ MWcm}^{-2}$) is no more than approximately a factor of 3 higher than that of photonic nanowire lasers ($\sim 5\text{-}20 \text{ MWcm}^{-2}$) of the same diameter, d [40]. In the deep-subwavelength region, where $d < 150 \text{ nm}$, in particular, the plasmonic nanolasers exhibit a much *smaller* threshold compared to their photonic counterparts, owing to the poor mode confinement and overlap with the gain medium for photonic nanolasers with $d < 150 \text{ nm}$. Finally, it should also be noted that the enhanced-SE rates in nanowire antennas also allows for higher laser-modulation speeds, which are predicted to exceed 1 THz [40], although this might come at the expense of Ohmic losses in the metal. To this end, initial experiments in zinc oxide (ZnO) plasmonic nanowire lasers have reported the observation of laser pulses shorter than 800 fs, suggesting a modulation bandwidth exceeding 1 THz [41] – perhaps the fastest laser reported to date.

4. Summary and outlook

Judiciously designed antenna nanostructures can give rise to dramatically enhanced spontaneous emission rates – by a factor of 300 having already been demonstrated – with good antenna efficiencies (above 50%) in some cases, and with broadband single-spatial-mode operation. A key idea in achieving this is to minimize the dissipated energy into the nanoantenna by suitable design of the nanostructure. Both, the visible [16, 35] and the near-infrared [22] regime appear to be suitable to that end. In principle, in addition to the standard metal-optics materials, gold and silver, one could also deploy alternative materials, such as refractory metals and metal nitrides [44, 45]. These alternative materials, which include W, Mo, TiN and ZrN, exhibit stiffer mechanical properties compared with Au or Ag. However, they also exhibit considerably higher optical losses and considerably lower thermal conductivity. For instance, the thermal conductivity of Au is $\sim 300 \text{ W/mK}$, whereas that of TiN is only $\sim 20 \text{ W/mK}$ [46]. Particularly on the nanoscale, this is a crucial issue because the resulting heat dissipation is not only a function of joule heat density (arising from absorption) but also a function of how quickly heat propagates away from the hot-spot. Thus, to achieve the same enhanced local field intensity, these alternative nanoantenna materials may have to experience one to two orders of magnitude higher operating temperatures, which would render them inferior to Au or Ag. Since these noble metals are anticipated to be considerably colder than their alternative counterparts, they may indeed continue to be (as they have been until now) more suitable for the herein discussed nanoscale light-emission and large field-enhancement applications.

Direct demonstrations of electrically modulated high-fluorescence devices with speeds exceeding 20 GHz is the next important step in the field. If successful, this may credibly lead to efficient, ultrafast LEDs eventually replacing lasers in very-short-distance microprocessing communications, reducing fabrication complexity and cost, and allowing for significant energy savings [4, 12, 21–23, 26].

Funding

U.S. Department of Energy (DE-AC02-05-CH11231); Canada Excellence Research Chairs Program; Max Planck Institute for the Science of Light (Eugen Lommel Fellowship); Center for Energy Efficient Electronics Science, National Science Foundation (NSF) (0939514).

Acknowledgments

This work was primarily funded by the Director, Office of Science, Office of Basic Energy Sciences, Materials Sciences and Engineering Division, of the U.S. Department of Energy under Contract No. DE-AC02-05-CH11231. The moving charge modeling was supported by the Canada Excellence Research Chairs Program, the Eugen Lommel fellowship of the Max Planck Institute for the Science of Light, Erlangen, Germany, and the Center for Energy Efficient Electronics Science, NSF Award 0939514.